Supplementary Data

Enhanced electrochemical performance of morphology-controlled titania-reduced graphene oxide nanostructures fabricated via combined anodization-hydrothermal process

Anitha V. C., ‡[a] Nazanin Hamnabard, ‡[a] Arghya Narayan Banerjee, [a*] Dillip G. R, [a] Sang Woo Joo[a*]

[a]School of Mechanical Engineering, Yeungnam University, Gyeongsan 712-749, South Korea

‡Authors contributed equally

*Corresponding authors

E-mail: banerjee_arghya@hotmail.com; arghya@ynu.ac.kr; Tel: +82-53-810-2453; Fax: +82-53-810-2062 (ANB)

E-mail: swjoo@yu.ac,kr; Tel: +82-53-810-3239; Fax: +82-53-810-2062 (SWJ)

Fig. S1: a) XRD patterns of RGO b) FE-SEM images of RGO and c) Raman spectra of RGO

Fig. S2: TEM images of (a) TNT, (top view of nanotube pore is shown in the inset), (b) TNR, (HR-TEM image of a single nanoribbon and corresponding d-spacing are shown in the inset), (c) TGNP and (d) TRGNF samples. Corresponding lower magnification images are shown in insets of (c)/(d) and the related d-spacings of TiO_2/GO/RGO are also indicated.

Fig. S3: a) UV-vis diffuse absorption of TNT and TRGNF samples b) corresponding Tauc's plot of the optical absorption.

Fig. S4: XPS survey spectra of a) TNT, b) TNR, c) TGNP and d) TRGNF.

Fig. S5: AFM images of (a) TNR, (b) TNT, (c) TGNP, (d) TRGNF, respectively.

Fig. S6: a) Cyclic voltammograms of GO and RGO on Ti foil at 10 mV/s, b) Specific capacitance as a function of the scan rate obtained from the CV data, c) Galvanostatic charge-discharge curves at 5 $\mu A/cm^2$, d) Specific capacitance as a function of the current densities obtained from the charge–discharge data and e) Ragone plots of power density versus energy density calculated from galvanostatic discharge for GO and RGO samples.

Fig. S1

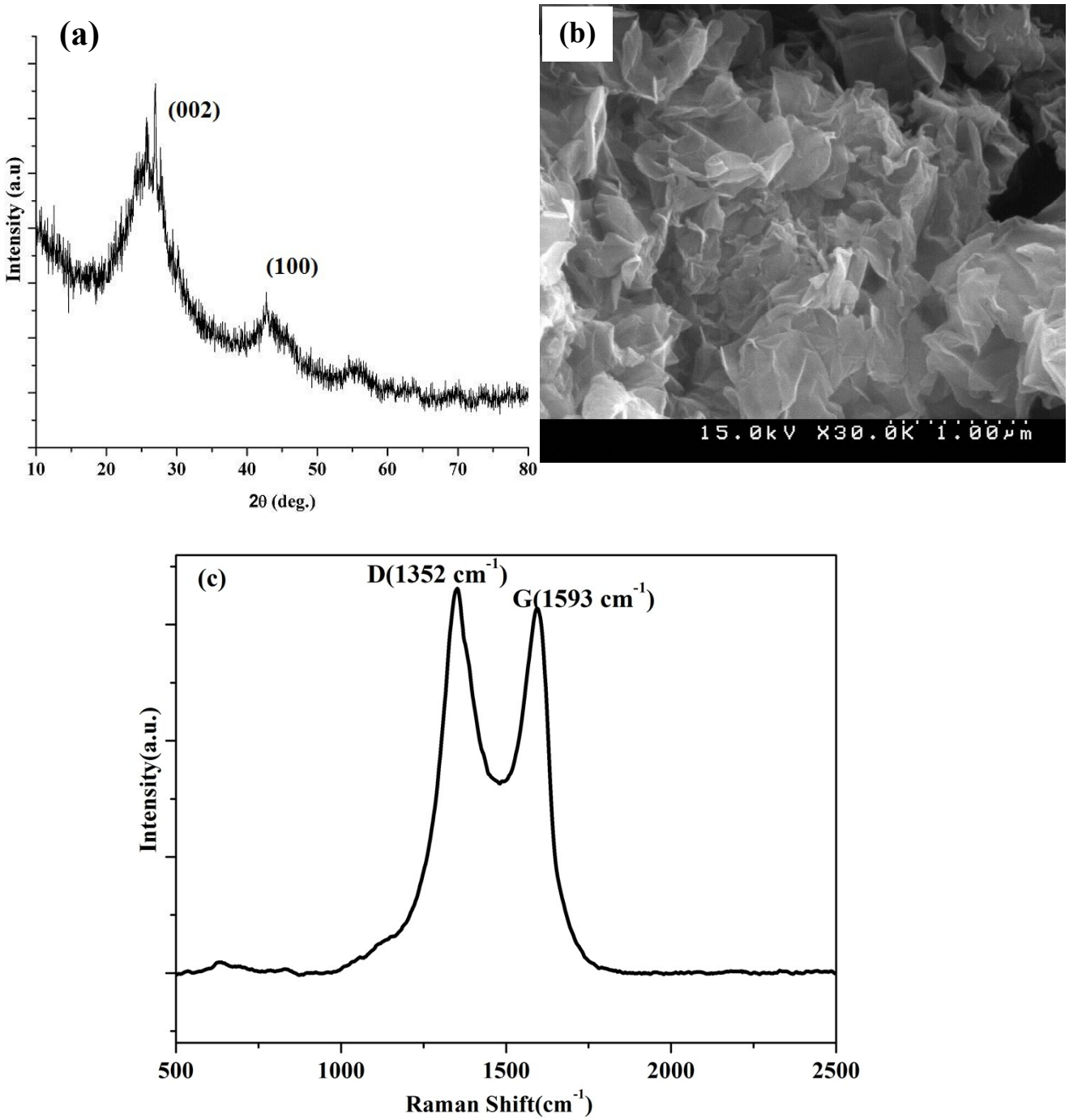

Fig. S1: a) XRD patterns of RGO b) FE-SEM images of RGO and c) Raman spectra of RGO

In Fig. S1(a), the XRD patterns of RGO, prepared using different reduction methods, exhibited two peaks, which are assigned to the diffraction peaks of (002) and (100) crystal planes of reduced graphene oxide. As shown in fig. S1(b), a crumpled and rippled structure is formed, which was the result of reduction of graphene oxide. So, the obtained results confirmed the reduction of GO in synthesis of TRGNF sample. The two main characteristic peaks D (1352 cm^{-1}) and G (1593 cm^{-1}) for RGO is evident in Fig.S1c

Fig.S2

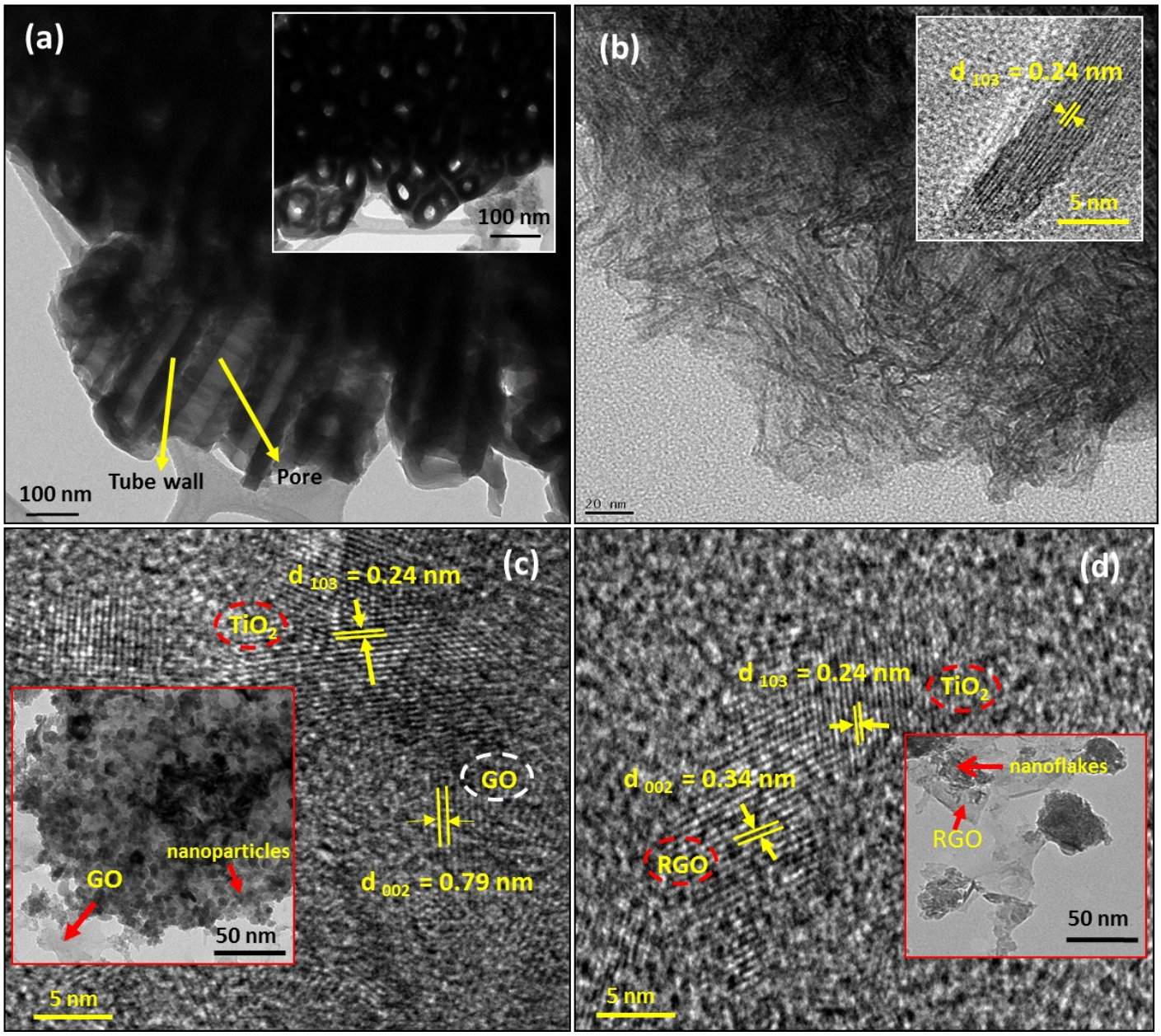

Fig. S2: TEM images of (a) TNT, (top view of nanotube pore is shown in the inset), (b) TNR, (HR-TEM image of a single nanoribbon and corresponding d-spacing are shown in the inset), (c) TGNP and (d) TRGNF samples. Corresponding lower magnification images are shown in insets of (c)/(d) and the related d-spacings of TiO_2/GO/RGO are also indicated.

Fig.S3

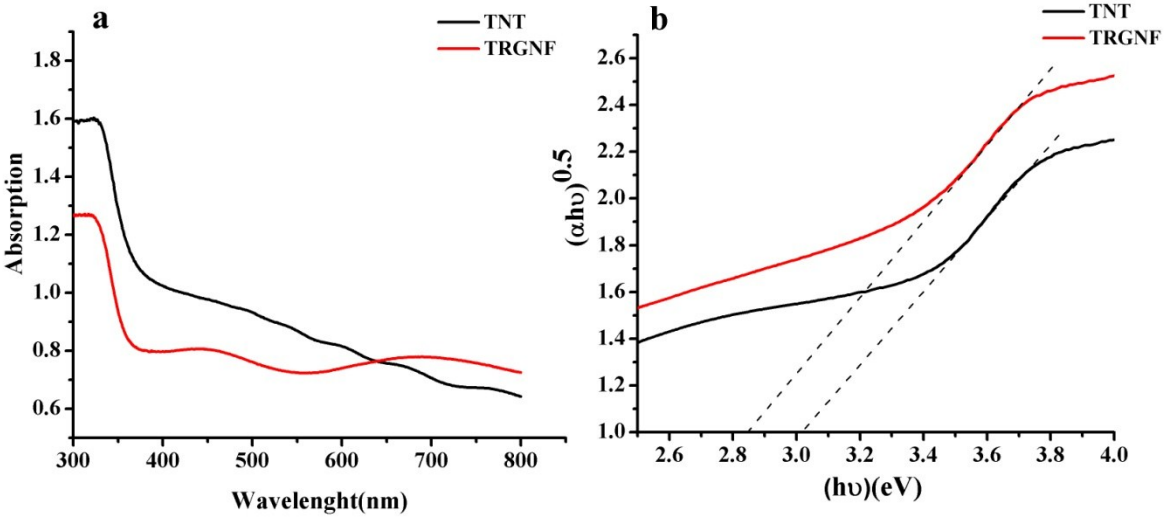

Fig. S3: a) UV-vis diffuse absorption of TNT and TRGNF samples b) corresponding Tauc's plot of the optical absorption.

Fig. S3(a) represents the UV-visible (UV–vis) absorption spectrum of TNT and TRGNF samples, confirming the interaction between TNT and reduced graphene oxide and helps to determine the possible change in band gap of titania-RGO nanoflakes composite. The red shift into the longer wavelength regions are occurred in the titania–RGO nanoflakes composite in absorption compared to bare titania nanotube. As shown in fig.S2(b), the optical band gaps of bare TNT and composite (TRGNF) samples were obtained using a Tauc plot of $(\alpha h\upsilon)^{1/2}$ versus $(h\upsilon)$ and by extrapolating an agent line generated from the linear region of the curve to the *x*-axis. The approximate band gaps of 3.02 eV and 2.85 eV are obtained for bare TNT and titania-RGO nanoflakes (TRGNF), respectively. The reported red shift can be attributed to a chemical interaction between TNT and RGO (may be resulted by formation of Ti-O-C chemical bonding) during the hydrothermal process and confirms the presence of RGO in TRGNF sample.

Fig.S4

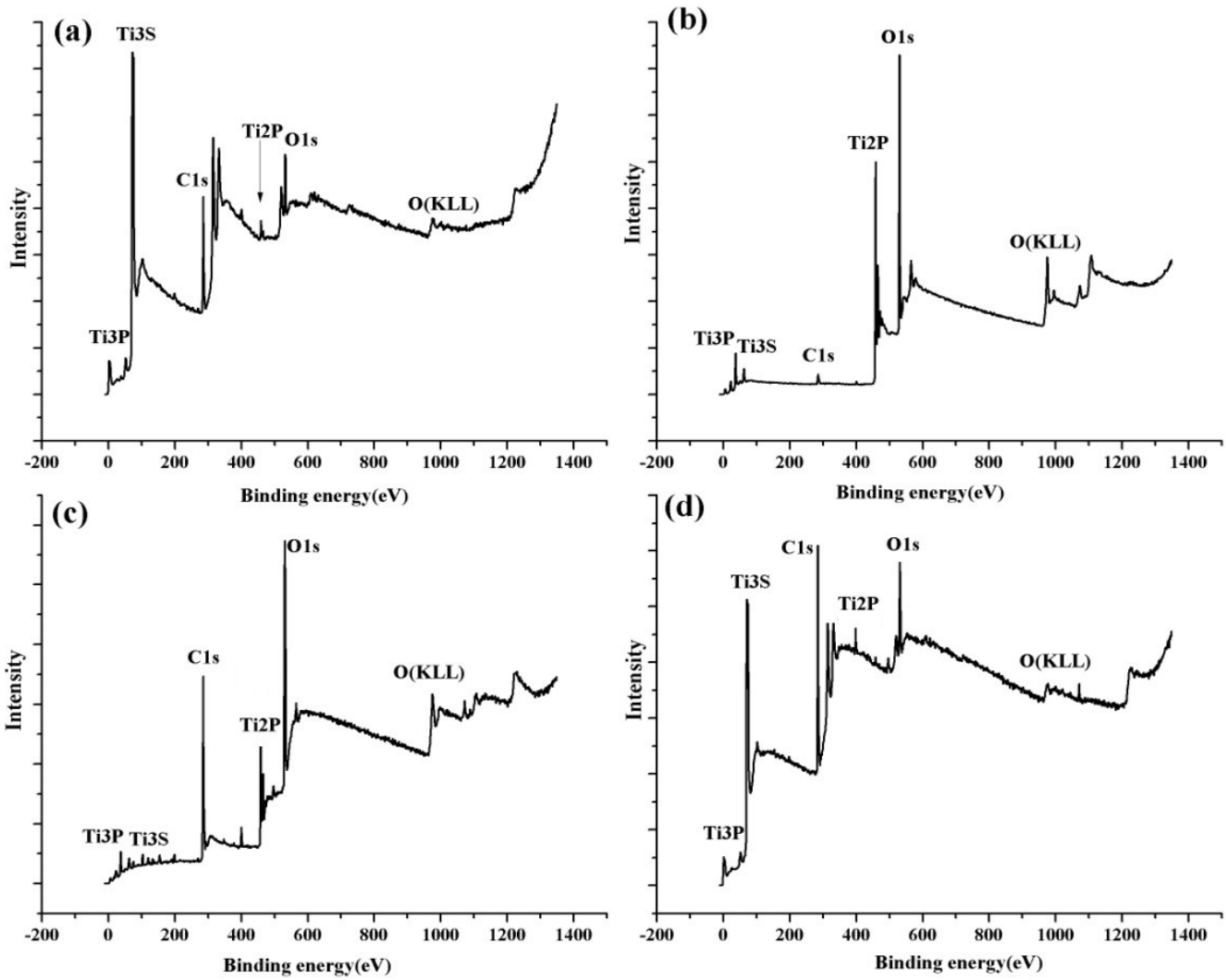

Fig. S4: XPS survey spectra of a) TNT, b) TNR, c) TGNP and d) TRGNF.

Fig.S5

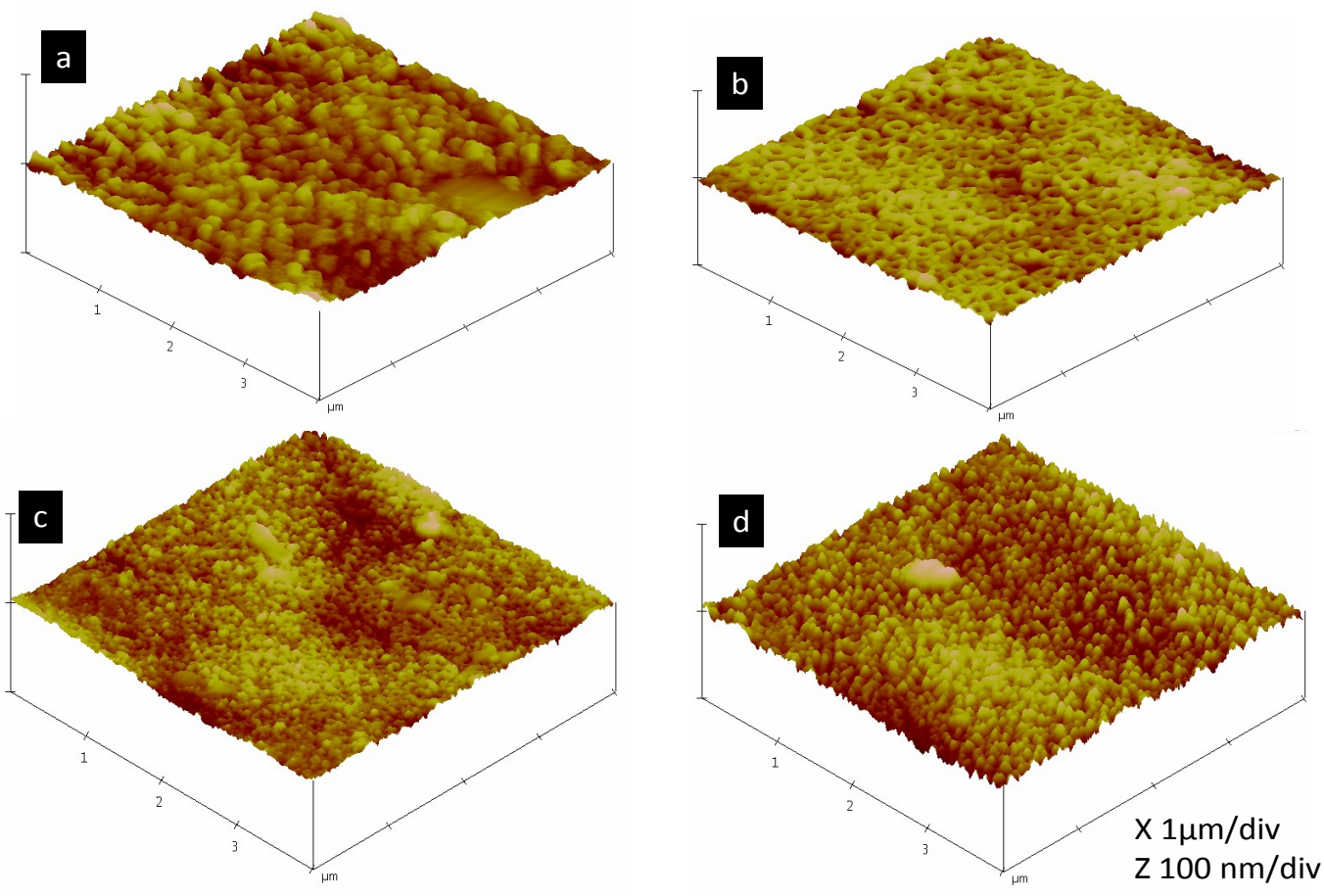

Fig.S5: AFM images of (a) TNR, (b) TNT, (c) TGNP, (d) TRGNF, respectively.

Fig.S6

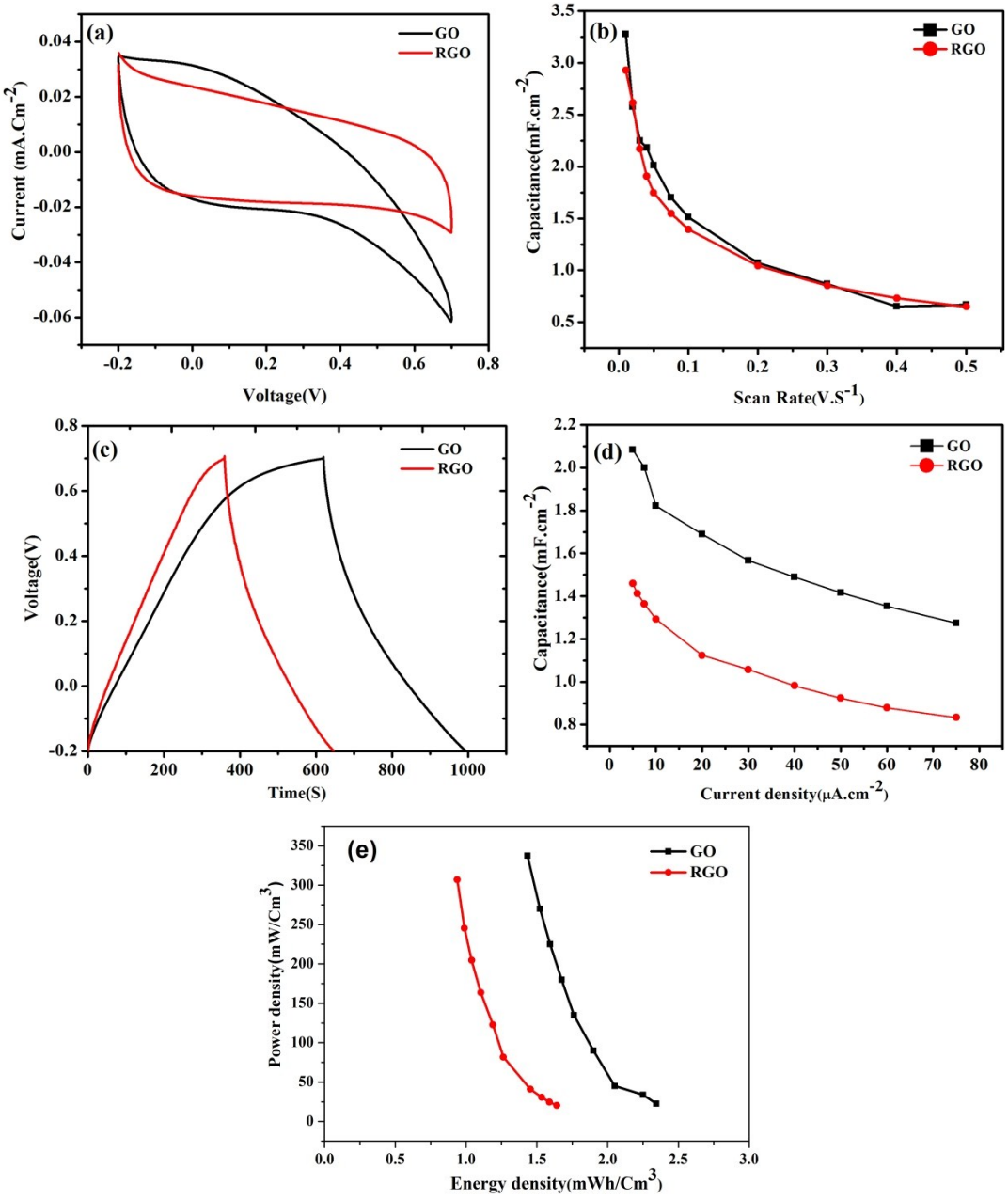

Fig. S6) a) Cyclic voltammograms of GO and RGO on Ti foil at 10 mV/s, b) Specific capacitance as a function of the scan rate obtained from the CV data, c) Galvanostatic charge-discharge curves at 5 μA/cm^2, d) Specific capacitance as a function of the current densities obtained from the charge–discharge data and e) Ragone plots of power density versus energy density calculated from galvanostatic discharge for GO and RGO samples.

Additionally, for a comparison study the capacitance, cycling stability and power density data of GO and RGO is plotted as Fig.S6. Fig.S6 (a) shows the cyclic voltammograms for GO and RGO on Ti foil in 1 M KCl solution in the range of -0.2 to +0.7 V (versus Ag/AgCl) at 10 mV/s. According to Eq. (1), the estimated specific capacitance of the GO is 3.2 $mF.cm^{-2}$ which is higher than RGO (2.9 $mF.cm^{-2}$) at 10 $mV.s^{-1}$. It can be noted from the CV curves that the specific capacitance of GO electrode is higher than that of the RGO electrode, suggesting that GO shows better electrochemical properties as shown in Fig. S6 (b).The galvanostatic charge/discharge is the most credible method to calculate the specific capacitance. As seen in Fig. S6(c), the charge–discharge performance of GO and RGO electrode is studied in 1 M KCl within a potential window of -0.2 to +0.7 V at a current density of 5 $\mu A.cm^{-2}$. The specific capacitances calculated from the charge–discharge profiles using equation (2), were 2.3 $mF.cm^{-2}$ for GO and 1.6 $mF.cm^{-2}$ for RGO, respectively. Also, Fig.S6 (d) indicates the variation and reduction of specific capacitance with current density. The results are in agreement with those calculated using cyclic voltammetry; however, the recorded values here are lower than those obtained using cyclic voltammetry. This improved specific capacitance of GO in comparison with RGO is due to the extra pseudo-capacitance effect of the attached oxygen-containing functional groups on its basal planes [1]. Additionally, the power density and energy density were calculated from the galvanostatic discharge curves using equations (6 and 7) are plotted in a Ragone diagram as Fig.S6 (e). As shown in the Ragone plots, the energy density of GO at a low power density of 22.5 mW cm^{-3} is 2.3 mW h cm^{-3}, higher than that of the RGO (1.64 mW h cm^{-3}) without much sacrifice power density.

References

1. B. Xu, S. Yue, Z. Sui, X. Zhang, S. Hou, G. Cao and Y. Yang, *Energy & Environmental Science*, 2011, **4**, 2826.